Optical anisotropy in optimally doped iron-based superconductor

npj | Quantum Materials

www.nature.com/npjquantmats

ARTICLE OPEN

Optical anisotropy in optimally doped iron-based superconductor

Anirban Pal[1], Manuel Chinotti[1], Jiun-Haw Chu[2,3,4], Hseuh-Hui Kuo[2,3], Ian Randal Fisher[2,3] and Leonardo Degiorgi[1]

The divergent nematic susceptibility, obeying a simple Curie-Weiss power law over a large temperature interval, is empirically found to be a ubiquitous signature in several iron-based materials across their doping-temperature phase diagram. The composition at which the associated Weiss temperature extrapolates to zero is found to be close to optimal doping, boosting the debate to what extent nematic fluctuations contribute to the pairing-mechanism and generally affect the electronic structure of iron-based superconductors. Here, we offer a comprehensive optical investigation of the optimally hole-doped $Ba_{0.6}K_{0.4}Fe_2As_2$ over a broad spectral range, as a function of temperature and of tunable applied stress, which acts as an external symmetry breaking field. We show that the stress-induced optical anisotropy in the infrared spectral range is reversible upon sweeping the applied stress and occurs only below the superconducting transition temperature. These findings demonstrate that there is a large electronic nematicity at optimal doping which extends right under the superconducting dome.

npj Quantum Materials (2019)4:3 ; https://doi.org/10.1038/s41535-018-0140-1

INTRODUCTION

The temperature-doping phase diagram of almost all iron-based superconductors (Fig. 1 for the hole doped materials) is characterized by an antiferromagnetic dome centered at the parent compound.[1,2] The onset of the magnetically ordered state below T_N is coincident with or follows a tetragonal-to-orthorhombic structural phase transition at $T_s(\geq T_N)$, that is driven by electronic nematic order. The latter breaks the tetragonal symmetry of the underlying lattice, without altering the translational symmetry.[2,3] Superconductivity emerges in proximity of such a broken symmetry state, at the bottom of the magnetic dome in both electron- and hole-doped systems (Fig. 1).

The in-plane *dc* resistivity anisotropy of the underdoped iron-based materials[4–7] was initially of paramount importance in shedding light on the origin of the structural phase transition within the concept of the electronic nematic order. In this context, the most important fingerprint is provided by the diverging nematic susceptibility in the tetragonal phase, as evinced by elastoresistance measurements (i.e., measurements of the induced resistivity anisotropy due to anisotropic strain).[8,9] Raman[10–12] and elastic moduli[13] investigations also point out the remarkable divergence of the nematic susceptibility. In a broader perspective, electronic nematicity is of relevance well beyond the iron-based superconductors since several cuprates and some heavy-fermion compounds, just to quote a few examples of other unconventional superconductors, do provide signatures for strongly anisotropic electronic phases.[14]

It has been empirically found,[15] that the divergent nematic susceptibility is a generic property of several iron-based superconductors even up to optimally doped compositions. This leads to the question of whether nematic quantum criticality could perhaps enhance the pairing interaction;[16–18] an intriguing possibility that has also been envisaged for the cuprates.[19,20] While the relationship between superconductivity and nematicity has been debated theoretically,[14] there remains a need to better experimentally scrutinize the influence of nematic fluctuations on the electronic properties over a large energy interval and also over a temperature (T) range extending under the superconducting dome, which is not accessible by elastoresistive technique.

Complementary to the *dc* transport data mostly affected by the energy scales close to the Fermi level, optical spectroscopy proves to be a powerful experimental tool in order to reveal the fingerprints of the nematic phase on the whole electronic structure.[21–29] In our experiment, we use uniaxial and in-situ tunable applied stress (p), which acts as a conjugate field to the orthorhombic distortion and allows circumventing sample twinning below T_s (see Supplementary Information). Above T_s, stress as external symmetry-breaking field induces a finite value of the orthorhombic distortion.[4] It is worth recalling that the microscopic mechanisms that result in the electronic anisotropy in the nematic phase are equivalent to those in the stressed tetragonal phase.[9,26,30] Consequently, measurements of the anisotropic optical response in stressed samples in the tetragonal phase (i.e., in the T-window where nematic fluctuations are involved) must directly connect to the electronic nematicity.[4,31] So far, optical investigations upon applying p have focused attention on the underdoped regime of the electron-doped 122 materials $Ba(Fe_{1-x}Co_x)_2As_2$ as well as on FeSe. The main motivation of this work is the study of the optimally doped regime (Fig. 1). To this purpose, we choose the hole-doped $Ba_{1-x}K_xFe_2As_2$, which displays a nematic state up to $x \sim 0.3$, when the antiferromagnetic phase boundary is reached.[32] Beyond this doping the nematic order disappears (i.e., $T_s = 0$), so that the optimally doped $x = 0.4$ compound is an ideal composition in order to address the impact

[1]Laboratorium für Festkörperphysik, ETH - Zürich, 8093 Zürich, Switzerland; [2]Geballe Laboratory for Advanced Materials and Department of Applied Physics, Stanford University, Stanford, CA 94305, USA and [3]Stanford Institute for Materials and Energy Sciences, SLAC National Accelerator Laboratory, 2575 Sand Hill Road, Menlo Park, CA 94025, USA
Correspondence: Leonardo Degiorgi (degiorgi@solid.phys.ethz.ch)
[4]Present address: Department of Physics, University of Washington, Seattle, WA 98103, USA

Received: 15 May 2018 Accepted: 5 December 2018
Published online: 10 January 2019

Published in partnership with Nanjing University

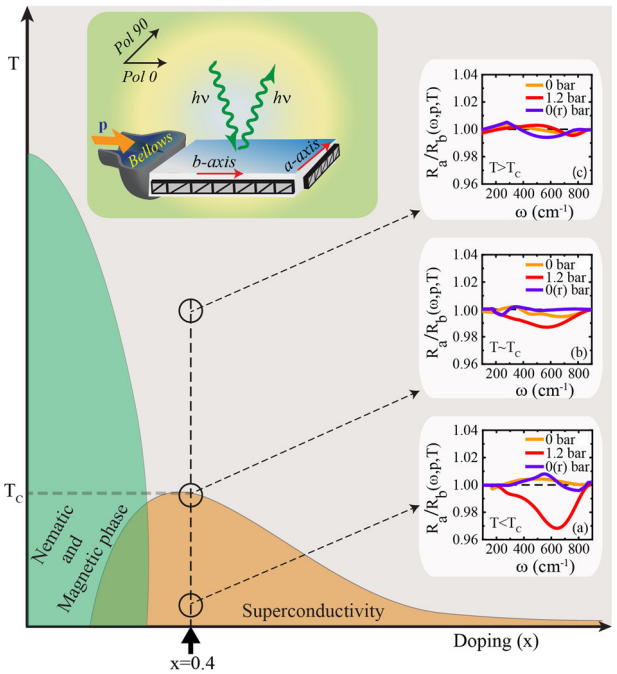

Fig. 1 Schematic view of the experiment and flavour of the major findings within the generic phase diagram of $Ba_{1-x}K_xFe_2As_2$: The optimally doped ($x = 0.4$ and $T_c = 38.5$ K) sample is illuminated with polarized light while external uniaxial compressive stress (p) is applied on the lateral face of the specimen. We adopt an experimental protocol consisting in the measurement of the optical reflectivity signal (R) during a p-loop after a zero-p-cooling (ZPC) procedure (see Methods as well as Supplementary Information).[24,25] We define the b-axis as the direction along which compressive p is applied and the a-axis as its orthogonal direction. Light is then polarized parallel to either axis (in the convention of our experimental set-up the polarization 0 is parallel to the b-axis and 90 to the a-axis). Below T_c (inset **a**) we clearly observe an anisotropy in the detected R-signal between the two axes when p is progressively applied, so that the ratio R_a/R_b deviates from 1 (i.e., isotropic limit). The ratios R_a/R_b are read from Fig. 2c at 0, at saturation (i.e., thick dotted line at 1.2 bar) and at 0 released p. R_a/R_b disappears upon releasing p back to zero ('(r)' denotes released p). At T_c (inset **b**) the onset of the optical anisotropy is only incipient and above T_c (inset **c**) there is no signature of the optical anisotropy upon sweeping p. We note that for compositions between $x \simeq 0.25$ and 0.3, $Ba_{1-x}K_xFe_2As_2$ suffers a reentrant C4 antiferromagnetic phase transition at temperatures below the C2 antiferromagnetic/nematic transition.[32] This aspect as well as the still on-going debate on the symmetry of the superconducting order parameter[1] are neglected in this schematic representation of the phase diagram

of the nematic fluctuations, imaged in our experiment by the p-induced anisotropy of the electrodynamic response.

RESULTS AND DISCUSSION

First of all, we offer a comprehensive view of the collected optical reflectivity ($R(\omega)$) data within the p-loop experiment at 10 K after a ZPC protocol (Fig. 1, and Methods section). The $R(\omega)$ spectra along the a- and b-axis, shown in Fig. 2a, b, are obviously metallic and approach total reflection at finite frequencies below $v_g \sim 180\,\mathrm{cm}^{-1}$, as expected at $T < T_c$. Further details about this experiment and additional data can be found in the Supplementary Information. While the discovery of the unprecedented p-induced anisotropy is at the center of our discussion, it is worthwhile to confirm the consistency of our data (averaged between the two axes) at all T with those in refs [33–38], which comprehensively address the optical signature of both normal and superconducting state in un-stressed $Ba_{1-x}K_xFe_2As_2$ samples (Fig. S1 in Supplementary Information). The reversible anisotropy upon sweeping p is already evident in the raw data and can be further emphasized by the calculation of the reflectivity ratio $R_{\mathrm{Ratio}} = R_a/R_b$, shown in Figs. 1a and 2c. R_{Ratio} drops below 1 (i.e., the isotropic situation) in the FIR range around $600\,\mathrm{cm}^{-1}$ upon reaching an applied p of 1.2 bar and reconverts to unity when p is released back to zero (see also Fig. 1a). The anisotropy is imaged in the real part $\sigma_1(\omega)$ of the optical conductivity as well, as shown in Fig. 2d,e. Particularly the so-called dichroism, defined as $\Delta\sigma_1(\omega) = \sigma_1^a(\omega) - \sigma_1^b(\omega)$ and depicted in Fig. 2f for the p-loop experiment at 10 K, allows the optical anisotropy to be resolved in the range between 300 and $1000\,\mathrm{cm}^{-1}$ for the stressed specimen, which further implies an anisotropy in the spectral weight distribution at FIR frequencies (Fig. S3 in Supplementary Information). Furthermore, we recognize the superconducting gap at 10 K for every p, identified by the drop of $\sigma_1(\omega)$ to almost zero below v_g, as illustrated in Fig. 2d, e) as well as Fig. 3b. Figures S1 and S2 in Supplementary Information for data at zero p and saturation, respectively, reinforce the gap opening at $T < T_c$. The sharp onset of absorption at about v_g in $\sigma_1(\omega)$ indicates a fully gapped superconducting material and the upturn of $\sigma_1(\omega)$ at frequencies towards zero accounts for the residual ungapped charge carriers (i.e., thermally activated across the gap) at finite T.

After having demonstrated that an optical anisotropy can be p-induced in the tetragonal structure of $Ba_{0.6}K_{0.4}Fe_2As_2$ at $T = 10\,\mathrm{K} < T_c$, we move to its T dependence and its relationship to the overall phase diagram of iron-based superconductors (Fig. 1). We first focus our attention on the quantity $\Delta R_{\mathrm{Ratio}}(\omega_0) = \frac{R_{\mathrm{Ratio}}(p=0,T) - R_{\mathrm{Ratio}}(p,T)}{R_{\mathrm{Ratio}}(p=0,T)} \times 100$, which amplifies the relative change of the optical anisotropy during the p-loop experiment at each T with respect to the $p = 0$ initial situation (i.e., the isotropic limit since $R_{\mathrm{Ratio}}(p = 0, T) \sim 1$ at all T) and helps truly pointing out the variation of the optical anisotropy beyond the experimental data noise. This latter quantity, read at the fixed frequency $\omega_0 = 600\,\mathrm{cm}^{-1}$, is shown in Fig. 3a. Our choice of ω_0 is motivated by the largest anisotropy (Fig. 2c) at that frequency. Even though there is a substantial Curie-like nematic susceptibility in the normal state (i.e., at $T > T_c$) from elastoresistive investigation,[15] our experiment does not have enough resolution in order to clearly recognize an optical anisotropy above T_c, which if any must be vanishingly small. It is however evident that the p-induced anisotropy develops upon entering the superconducting state at applied p large enough to cause a polarization dependence of the excitation spectrum. At saturation (thick horizontal dotted line at $p = 1.2$ bar) the color map in Fig. 3a reveals the pronounced increase of the optical anisotropy only at $T < T_c$. This is evidence for the growing of the p-induced nematicity even in the superconducting state, despite the established hardening occurring below T_c[13] and the mild reduction at low T of the Raman susceptibilities[11] for dopings across the whole phase diagram. Indeed, the discovered optical anisotropy is in contrast to expectations based solely on anticipated strain for a fixed stress; because of the hardening on cooling beneath T_c, a fixed stress would cause a smaller strain and thus an anisotropy of the optical response getting smaller upon cooling through T_c. On the contrary, we observe the opposite. The T evolution of the optical anisotropy is also mapped by $\Delta\sigma_1(\omega)$, as shown in the energy interval between 200 and $1000\,\mathrm{cm}^{-1}$ at three selected p in Fig. 3c–e. These panels again highlight the p-induced as well as p-reversible optical anisotropy below T_c in the FIR range. This is the most important results of this work, signaling the presence of electronic nematicity at T deep into the superconducting dome and that the band structure is responding to nematic fluctuations.

Before going any further and in order to set the stage for our conclusions, it is instructive to briefly recall our previous optical findings with respect to the nematic phase in the underdoped

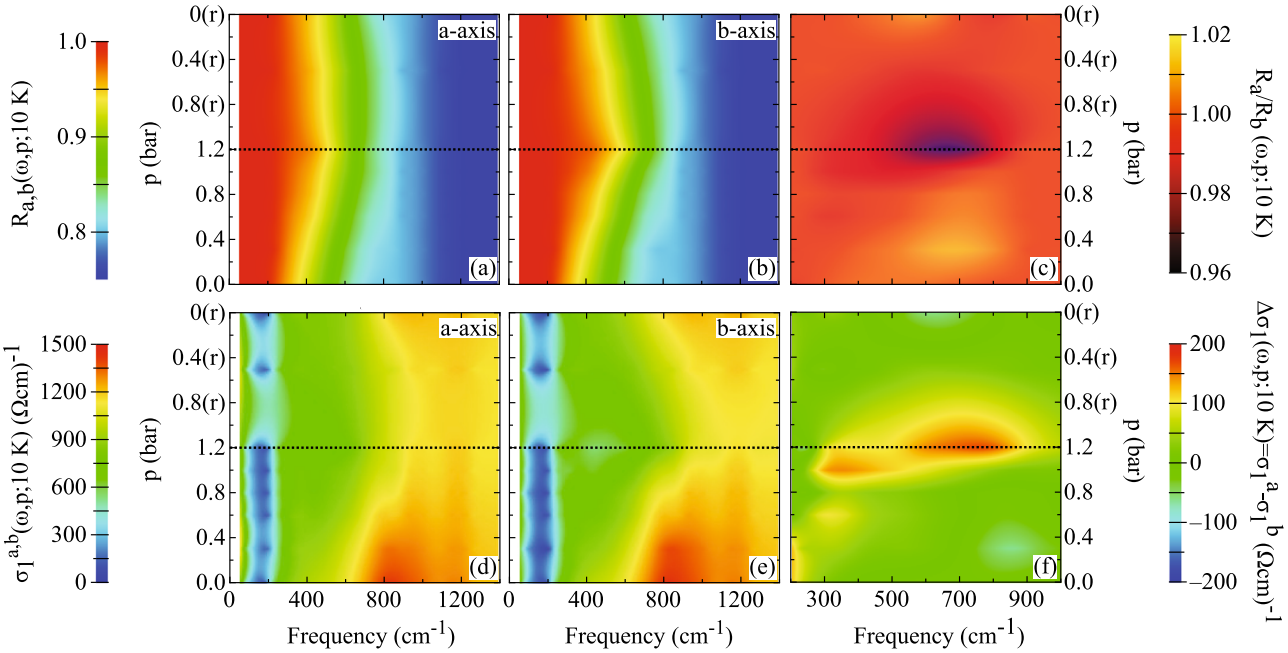

Fig. 2 Stress dependence of the optical anisotropy of $Ba_{0.6}K_{0.4}Fe_2As_2$ at $T < T_c$: **a**, **b** Representative data of the optical reflectivity ($R(\omega)$) at 10 K for the *p*-loop experiment after a ZPC protocol along the *a*- and *b*-axis (R_a and R_b, respectively, Fig. 1) in the spectral range below 1400 cm^{-1}. **c** The reflectivity ratio $R_{Ratio} = R_a/R_b$. **d**, **e** Real part $\sigma_1(\omega)$ of the optical conductivity, achieved through KK transformation of the data in panels **a** and **b**. **f** The so-called dichroism $\Delta\sigma_1(\omega) = \sigma_1^a(\omega) - \sigma_1^b(\omega)$ at 10 K within the *p*-loop experiment. **c**, **f** focus the attention to the FIR energy interval 200–1000 cm^{-1}, where the reversible optical anisotropy upon sweeping *p* is discovered. A first-neighbor interpolation procedure is used in order to generate the color maps. Released pressures are denoted by '(r)'. The thick dotted line in all panels marks $p = 1.2$ bar (i.e., at saturation)

regime of $Ba(Fe_{1-x}Co_x)_2As_2$.[24–27] At $T < T_s$ ($= 135$ K for the parent compound and decreasing upon Co-doping[1,4]), the optical anisotropy exhibits a remarkable hysteretic response to the applied *p* even at energies pertinent to the electronic structure, within 0.3 eV from the Fermi level (Fig. 3 in ref. [25]). Referring to $R_{Ratio}(\omega_0)$ as a representative quantity for the optical anisotropy, the largest one at saturation was identified at $\omega_0 \sim 1500$ cm^{-1} for the parent compound, being of the order of 5% at the lowest investigated *T* and decreasing to values of about 3% for $T \to T_s$. The optical anisotropy at saturation for $T < T_s$ decreases upon doping in the underdoped regime, showing a correlation with the Co-doping dependence of the orthorhombicity (Fig. 4 in ref. [25]). The anisotropy at ω_0 turns into a reversible linear *p* dependence at $T \geq T_s$, further decreasing to values of about 1–3% at the highest applied stress (Fig. 3 in ref. [25]). Our results indicate an important polarization of the electronic structure in the nematic phase below T_s and a significant *p*-induced one above T_s. The hysteretic behavior was also revealed in the optical anisotropy of FeSe at $T < T_s (= 90$ K) with $\omega_0 \sim 1000$ and 3000 cm^{-1},[28,29] among which even a change of sign occurs in the polarization dependence of the measured spectra (Fig. 2 in ref. [28]). The magnitude of the optical anisotropy itself is comparable to the values discovered in the underdoped regime of Co-doped 122 materials. However, the optical anisotropy at ω_0 in FeSe displays a rather sudden drop on approaching T_s from low *T*. We conclude that the anticipated *p*-induced lattice distortion above T_s in FeSe may be less strongly or not obviously bound to the electronic structure as in other iron-based superconductors.[28,29] Common to both families of Co-underdoped 122 and FeSe is nonetheless the persistence even at $T < T_c$ of the optical anisotropy evinced in the nematic phase, so that superconductivity develops in an electronically polarized state.[26–29] Overall, the anisotropy in the optical response at mid-infrared energy scales unfolded in $Ba(Fe_{1-x}Co_x)_2As_2$ and FeSe signals the impact of the nematic phase to all iron *d* orbitals (squeezed in energy by correlation effects) and highlights the relevance of the orbital degree of freedom, as advanced by photoemission data.[31,39–44] Such an anisotropic optical response at mid-infrared energy scales originates from the split of the relevant bands of the order of only a few tens of meV.[39]

Our present data of the optimally doped $Ba_{0.6}K_{0.4}Fe_2As_2$ bear testimony to a *p*-induced anisotropy of the excitation spectrum in the purely tetragonal phase, which is reversible upon applying and releasing *p*, respectively. Therefore, an anisotropy in the charge dynamics due to (*p*-induced) nematicity[24–27] seems to be a generic feature in 122 iron-based superconductors even into the optimally-doped regime, similar to the *dc* transport properties.[15] Somehow peculiar with respect to the previously investigated underdoped 122 materials and even FeSe,[24–29] the optical anisotropy in the optimally K-doped 122 compound occurs at the much lower FIR energy scales, relevant to the superconducting gap(s) (Figs. 1a–c, 2f and 3c–e), thus excluding the involvement of bands deep into the electronic structure and possibly implying a less prominent impact of orbital ordering in the optimally doped than in the underdoped regime. While the different electronic structures between the various families of iron-based superconductors cannot be neglected a priori with respect to the anisotropic excitation spectrum, those (low) energy scales, at which the *p*-induced optical anisotropy occurs in $Ba_{0.6}K_{0.4}Fe_2As_2$, are possibly related to the response of the conduction bands to an external symmetry breaking field. The excitation spectrum of the itinerant charge carriers at the energy scales close to the Fermi level, ultimately of relevance for the transport properties as well as superconductivity, could be affected by *p*-induced anisotropic scattering. Precisely such (anisotropic) scattering may uncover some kind of spin-orbital interplay, where for instance the *p*-induced nematicity is caused by spin fluctuations and is vestigial to stripe magnetism.[16] Alternatively, an external symmetry breaking field, like uniaxial stress, leads to a so-called differentiation of the orbital effective masses, which is even further enhanced by the presence of strong electron correlations.[45] Indeed, the latter

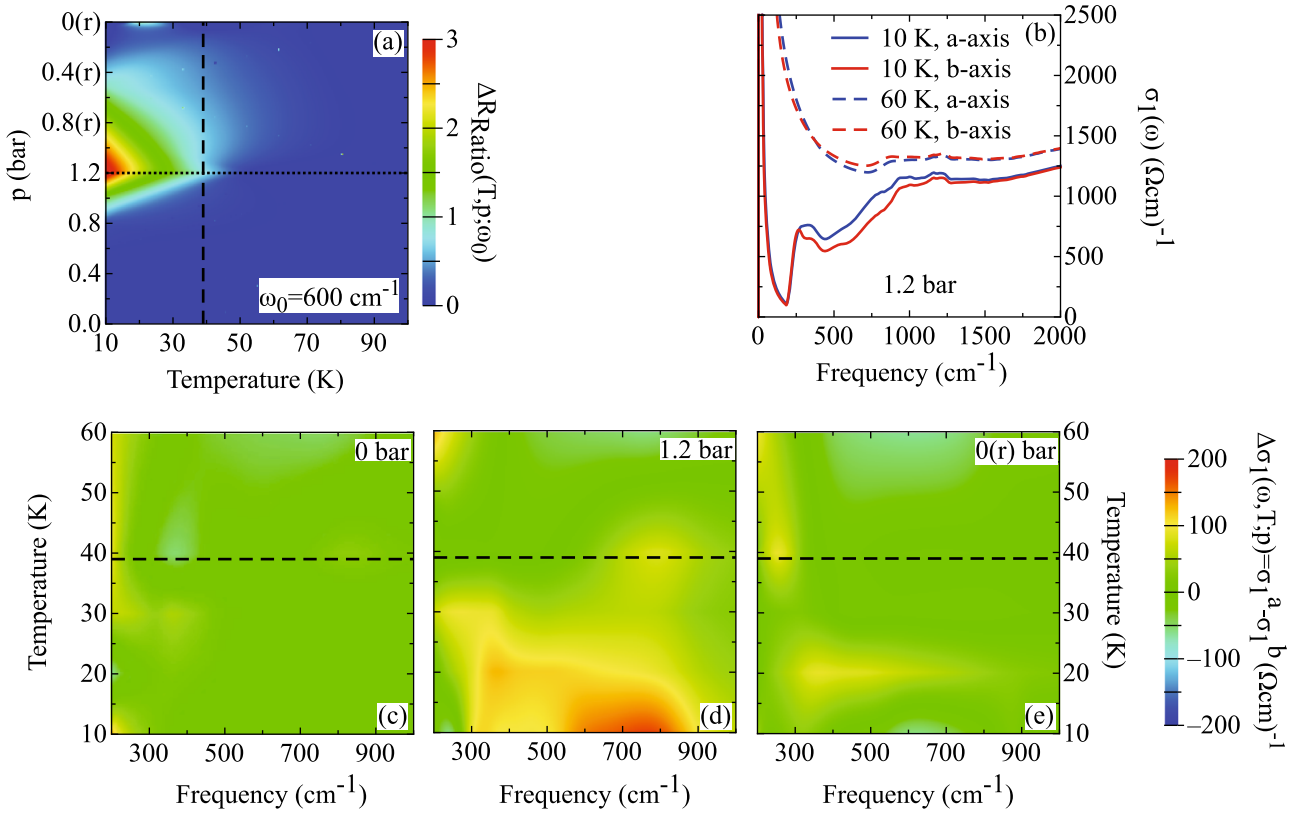

Fig. 3 Temperature dependence of the anisotropic optical response of $Ba_{0.6}K_{0.4}Fe_2As_2$ upon applying stress: **a** T dependence of the quantity $\Delta R_{Ratio}(\omega_0)$ (see text) within the p-loop experiment after a ZPC protocol, which emphasizes the T evolution of the p-induced optical anisotropy. We choose $\omega_0 = 600\ cm^{-1}$. **b** Measured $\sigma_1(\omega)$ at 10 K and 60 K for $p = 1.2$ bar along both crystallographic axes. **c**–**e** T dependence of $\Delta\sigma_1(\omega)$ at the selected p of 0, 1.2 and released 0 bar. These panels focus the attention to the FIR energy interval 200–1000 cm^{-1}, thus emphasising the reversible optical anisotropy upon sweeping p. The thick dashed line in all panels indicates T_c. A first-neighbor interpolation procedure is used in order to generate the color maps. Released pressures are denoted by '(r)'

are supposed to be pronounced in hole-doped materials. Anisotropic effective masses affect the optical response of the conduction bands as well. This could be also reflected by an anisotropic reshuffling of spectral weight at $T < T_c$ between the superconducting collective mode and the FIR energies (Fig. 3c–e), as elaborated in Fig. S3 in Supplementary Information.

In conclusion, the discovery of such an unprecedented p-induced optical anisotropy in (optimally doped) $Ba_{0.6}K_{0.4}Fe_2As_2$ only at $T < T_c$ (Figs. 1a–c and 3a) suggests that its electronic structure is extremely susceptible to symmetry breaking stress below T_c. This may shed new light on the putative relationship between quantum critical nematic fluctuations and unconventional superconductivity.[18,19] In this respect, establishing the exact extent to which uniaxial stress couple to nematic fluctuations (i.e., at $T > T_s \sim 0$) is of paramount importance and is a challenge left to the future.

METHODS

The large single crystals of $Ba_{0.6}K_{0.4}Fe_2As_2$ ($T_c = 38.5$ K) for this study were grown using a self-flux method, as described previously[46] (see Supplementary Information). The tunable stress (p) is applied with our custom-made mechanical device, thoroughly described in refs [24,25]. It consists of a spring bellows, which can be extended or retracted by flushing He-gas into its volume or evacuating it, thus exerting or releasing uniaxial p on the lateral side of the specimen (Fig. 1), respectively. As in refs [24,25], we refer here to the He-gas pressure inside the volume of the bellows ($p_{bellows}$): the effective stress felt by the sample (p_{sample}) depends on its size and thickness, so that $p_{bellows} = 0.1$ bar corresponds to an effective uniaxial stress of about $P_{sample} \sim 2.5$ MPa on our crystals. It has been widely established that an effective stress of at least 10 MPa is enough to reveal the underlying symmetry-breaking.[4]

The optical reflectivity $R(\omega)$ as a function of temperature (T) and p is measured at nearly normal incidence[47] with the electromagnetic radiation polarized along the a- ($R_a(\omega)$) and b- ($R_b(\omega)$) axis (Fig. 1) from the far-infrared (FIR) up to the ultra-violet. We discuss here data collected after the zero-pressure-cooled (ZPC) protocol.[24,25] At the target T achieved with $p = 0$, stress was first increased step-wise from 0 to 1.2 bar (above which a saturation of the (anisotropic) optical response for $T < T_c$ has been found) and then decreased back to zero, thus completing the p-loop. We use a different stress grid upon increasing and decreasing p. This could lead to some tiny data asymmetry along the p-loop within the first-neighbor interpolation procedure used in order to generate the color maps in the figures. The real part $\sigma_1(\omega)$ of the optical conductivity was obtained via the Kramers-Kronig (KK) transformation of $R(\omega)$ by applying suitable extrapolations at low and high frequencies (see Supplementary Information).[47]

DATA AVAILABILITY

The data that support the findings of this study are available from the corresponding author upon reasonable request.

ACKNOWLEDGEMENTS

We wish to thank R. Fernandes, M. Schütt, R. Lobo, L. Benfatto, L. Fanfarillo, B. Valenzuela, E. Bascones, A. Chubukov, P. Hirschfeld, W. Ku, and D. Lu for fruitful discussions. This work was supported by the Swiss National Science Foundation (SNSF). Work at Stanford University was supported by the Department of Energy, Office of Basic Energy Sciences under contract DE-AC02-76SF00515.

AUTHOR CONTRIBUTIONS

L.D. and I.R.F. conceived the experiment. A.P. and M.C. carried out the optical experiments and participated in the analysis, figure planning, and draft preparation,

which was completed with input from all the authors. J.H.C., H.H.K., and I.R.F. supplied the specimen. The project was supervised by L.D.

ADDITIONAL INFORMATION

Supplementary information accompanies the paper on the *npj Quantum Materials* website (https://doi.org/10.1038/s41535-018-0140-1).

Competing interests: The authors declare no competing interests.

Publisher's note: Springer Nature remains neutral with regard to jurisdictional claims in published maps and institutional affiliations.

REFERENCES

1. Paglione, J. & Greene, R. L. High-temperature superconductivity in iron-based materials. *Nat. Phys.* **6**, 645–658 (2010).
2. Fernandes, R. M., Chubukov, A. V. & Schmalian, J. What drives nematic order in iron-based superconductors? *Nat. Phys.* **10**, 97–104 (2014).
3. Fradkin, E., Kivelson, S. A., Lawler, M. J., Eisenstein, J. P. & Mackenzie, A. P. Nematic Fermi fluids in condensed matter physics. *Annu. Rev. Condens. Matter Phys.* **1**, 153–178 (2010).
4. Fisher, I. R., Degiorgi, L. & Shen, Z. X. In-plane electronic anisotropy of underdoped 122 Fe-arsenide superconductors revealed by measurements of detwinned single crystals. *Rep. Prog. Phys.* **74**, 124506 (2011).
5. Chu, J.-H. et al. In-plane resistivity anisotropy in an underdoped iron arsenide superconductor. *Science* **329**, 824–826 (2010).
6. Blomberg, E. C. et al. In-plane anisotropy of electrical resistivity in strain-detwinned $SrFe_2As_2$. *Phys. Rev. B* **83**, 134505 (2011).
7. Blomberg, E. C. et al. Effect of tensile stress on the in-plane resistivity anisotropy in $BaFe_2As_2$. *Phys. Rev. B* **85**, 144509 (2012).
8. Chu, J.-H., Kuo, H.-H., Analytis, J. G. & Fisher, I. R. Divergent nematic susceptibility in an iron arsenide superconductor. *Science* **337**, 710–712 (2012).
9. Kuo, H. H., Shapiro, M. C., Riggs, S. C. & Fisher, I. R. Measurement of the elastoresistivity coefficients of the underdoped iron arsenide $Ba(Fe_{0.975}Co_{0.025})_2As_2$. *Phys. Rev. B* **88**, 085113 (2013).
10. Gallais, Y. et al. Observation of incipient charge nematicity in $Ba(Fe_{1-x}Co_x)_2As_2$. *Phys. Rev. Lett.* **111**, 267001 (2013).
11. Wu, S.-F. et al. Superconductivity and electronic fluctuations in $Ba_{1-x}K_xFe_2As_2$ studied by Raman scattering. *Phys. Rev. B* **95**, 085125 (2017).
12. Wu, S.-F. et al. On the origin of critical nematic fluctuations in pnictide superconductors. http://arxiv.org/abs/1712.06066 (2017).
13. Böhmer, A. E. et al. Nematic susceptibility of hole-doped and electron-doped $BaFe_2As_2$ iron-based superconductors from shear modulus measurements. *Phys. Rev. Lett.* **112**, 047001 (2014).
14. Fradkin, E., Kivelson, S. A. & Tranquada, J. M. Colloquium: theory of intertwined orders in high temperature superconductors. *Rev. Mod. Phys.* **87**, 457–482 (2015).
15. Kuo, H.-H., Chu, J.-H., Palmstrom, J. C., Kivelson, S. A. & Fisher, I. R. Ubiquitous signatures of nematic quantum criticality in optimally doped Fe-based superconductors. *Science* **352**, 958–962 (2016).
16. Chubukov, A. V., Khodas, M. & Fernandes, R. M. Magnetism, superconductivity, and spontaneous orbital order in iron-based superconductors: which comes first and why? *Phys. Rev. X* **6**, 041045 (2016).
17. Metlitski, M. A., Mross, D. F., Sachdev, S. & Senthil, T. Cooper pairing in non-Fermi liquids. *Phys. Rev. B* **91**, 115111 (2015).
18. Lederer, S., Schattner, Y., Berg, E. & Kivelson, S. A. Enhancement of superconductivity near a nematic quantum critical point. *Phys. Rev. Lett.* **114**, 097001 (2015).
19. Nie, L., Tarjus, G. & Kivelson, S. A. Quenched disorder and vestigial nematicity in the pseudogap regime of the cuprates. *Proc. Natl Acad. Sci. USA* **111**, 7980–7985 (2014).
20. Fujita, K. et al. Simultaneous transitions in cuprate momentum-space topology and electronic symmetry breaking. *Science* **344**, 612–616 (2014).
21. Nakajima, M. et al. Unprecedented anisotropic metallic state in undoped iron arsenide $BaFe_2As_2$ revealed by optical spectroscopy. *Proc. Natl Acad. Sci. USA* **108**, 12238–12242 (2011).
22. Nakajima, M. et al. Effect of Co doping on the in-plane anisotropy in the optical spectrum of underdoped $Ba(Fe_{1-x}Co_x)_2As_2$. *Phys. Rev. Lett.* **109**, 217003 (2012).
23. Ishida, S. et al. Anisotropy of the in-plane resistivity of underdoped $Ba(Fe_{1-x}Co_x)_2As_2$ superconductors induced by impurity scattering in the antiferromagnetic orthorhombic phase. *Phys. Rev. Lett.* **110**, 207001 (2013).
24. Mirri, C. et al. Hysteretic behavior in the optical response of the underdoped Fe-arsenide $Ba(Fe_{1-x}Co_x)_2As_2$ in the electronic nematic phase. *Phys. Rev. B* **89**, 060501(R) (2014).
25. Mirri, C. et al. Nematic-driven anisotropic electronic properties of underdoped detwinned $Ba(Fe_{1-x}Co_x)_2As_2$ revealed by optical spectroscopy. *Phys. Rev. B* **90**, 155125 (2014).
26. Mirri, C. et al. Origin of the resistive anisotropy in the electronic nematic phase of $BaFe_2As_2$ revealed by optical spectroscopy. *Phys. Rev. Lett.* **115**, 107001 (2015).
27. Mirri, C. et al. Electrodynamic response in the electronic nematic phase of $BaFe_2As_2$. *Phys. Rev. B* **93**, 085114 (2016).
28. Chinotti, M., Pal, A., Degiorgi, L., Böhmer, A. E. & Canfield, P. C. Optical anisotropy in the electronic nematic phase of FeSe. *Phys. Rev. B* **96**, 121112(R) (2017).
29. Chinotti, M., Pal, A., Degiorgi, L., Böhmer, A. E. & Canfield, P. C. Ingredients for the electronic nematic phase in FeSe revealed by its anisotropic optical response. *Phys. Rev. B* **98**, 094506 (2018).
30. Kuo, H.-H. & Fisher, I. R. Effect of disorder on the resistivity anisotropy near the electronic nematic phase transition in pure and electron-doped $BaFe_2As_2$. *Phys. Rev. Lett.* **112**, 227001 (2014).
31. Yi, M. et al. Symmetry-breaking orbital anisotropy observed for detwinned $Ba(Fe_{1-x}Co_x)_2As_2$ above the spin density wave transition. *Proc. Natl Acad. Sci. USA* **108**, 6878–6883 (2011).
32. Böhmer, A. E. et al. Superconductivity-induced re-entrance of the orthorhombic distortion in $Ba_{1-x}K_xFe_2As_2$. *Nat. Commun.* **6**, 7911 (2015).
33. Li, G. et al. Probing the superconducting energy gap from infrared spectroscopy on a $Ba_{0.6}K_{0.4}Fe_2As_2$ single crystal with $T_c = 37$ K. *Phys. Rev. Lett.* **101**, 107004 (2008).
34. Charnukha, A. et al. Eliashberg approach to infrared anomalies induced by the superconducting state of $Ba_{0.68}K_{0.32}Fe_2As_2$ single crystals. *Phys. Rev. B* **84**, 174511 (2011).
35. Charnukha, A. et al. Superconductivity-induced optical anomaly in an iron arsenide. *Nat. Commun.* **2**, 219 (2011).
36. Dai, Y. M. et al. Hidden T-linear scattering rate in $Ba_{0.6}K_{0.4}Fe_2As_2$ revealed by optical spectroscopy. *Phys. Rev. Lett.* **111**, 117001 (2013).
37. Dai, Y. M. et al. Optical conductivity of $Ba_{0.6}K_{0.4}Fe_2As_2$: the effect of in-plane and out-of-plane doping in the superconducting gap. *EPL* **104**, 47006 (2013).
38. Xu, B. et al. Infrared probe of the gap evolution across the phase diagram of $Ba_{1-x}K_xFe_2As_2$. *Phys. Rev. B* **96**, 115125 (2017).
39. Yi, M., Zhang, Y., Shen, Z.-X. & Lu, D. Role of the orbital degree of freedom in iron-based superconductors. *npj Quantum Mater.* **2**, 57 (2017).
40. Yi, M. et al. Electronic reconstruction through the structural and magnetic transitions in detwinned NaFeAs. *N. J. Phys.* **14**, 073019 (2012).
41. Wang, Q. et al. Symmetry-broken electronic structure and uniaxial Fermi surface nesting of untwinned $CaFe_2As_2$. *Phys. Rev. B* **88**, 235125 (2013).
42. Fanfarillo, L. et al. Orbital-dependent Fermi surface shrinking as a fingerprint of nematicity in FeSe. *Phys. Rev. B* **94**, 155138 (2016).
43. Watson, M. D. et al. Formation of Hubbard-like bands as a fingerprint of strong electron-electron interactions in FeSe. *Phys. Rev. B* **95**, 081106(R) (2017).
44. Evtushinsky, D. V. et al. Direct observation of dispersive lower Hubbard band in iron-based superconductor FeSe. http://arxiv.org/abs/1612.02313 (2016).
45. Fanfarillo, L., Giovannetti, G., Capone, M. & Bascones, E. Nematicity at the Hund's metal crossover in iron superconductors. *Phys. Rev. B* **95**, 144511 (2017).
46. Chu, J.-H., Analytis, J. G., Kucharczyk, C. & Fisher, I. R. Determination of the phase diagram of the electron-doped superconductor $Ba(Fe_{1-x}Co_x)_2As_2$. *Phys. Rev. B* **79**, 014506 (2009).
47. Dressel, M. & Grüner, G. *Electrodynamics of Solids*. (Cambridge University Press, Cambridge, England, 2002).